GROUND LATERAL SPREAD EFFECTS ON SINGLE PILE USING UNCOUPLED ANALYSIS METHOD

San-Shyan Lin[1], Yu-Ju Tseng[2], Jen-Cheng Liao[3], C.H. Wang[3], and Wei F. Lee[4]

ABSTRACT

Permanent ground deformation or ground lateral spreading is observed to be the main cause for the distress of piles embedded in liquefied ground. The purpose of this paper is to use uncoupled method for analysis of ground lateral spread effect on piles. The computer code, CYCLIC-1D (Elgamal, *et al*., 2002) developed at University of California at San Diego and accessible from the web, is used for lateral ground deformation estimation. Subsequently, the pile performance, treated as beam on Winkler foundation, is studied considering the effect of ground deformation obtained from CYCLIC-1D. Three centrifuge tested examples and one real field case were studied by the aforementioned method. Reasonable agreement was obtained between the predicted and the measured results.

Key words: Pile, lateral spreading, soil liquefaction.

1. INTRODUCTION

It is known that the effects of liquefaction on piles are often damaging. The lateral spreading usually is triggered at the slightly inclined slope with liquefiable soils embedded among the soil layers. When the soil liquefaction was initiated, the liquefied soils tend to slide downward along the inclined surface. While the pile is embedded among these moving liquefiable soils, the pile can sustain lateral force caused by the liquefied soils. Serious structural damages can be produced, such as the 1964 Niigata earthquake (Hamada, 1992), the 1995 Kobe earthquake (Tokimatsu, 2003) and the 1999 Chi-Chi earthquake (Hwang, *et al*. 2003) had left extensive damage to many pile foundations of bridges and buildings.

Bhattacharya, *et al*. (2004) proposed an alternative mechanism of pile failure in liquefiable deposits during earthquakes. It was considered that the pile becomes unstable under axial load from loss of support from the surrounding liquefied soil, provided the slenderness ratio of the pile in the unsupported zone exceeds a critical value. The instability causes the pile to buckle and cause a plastic hinge in the pile. In terms of soil pile interaction, the method assumes that, during instability, the pile pushes the soil. Hence, the lateral load effects are considered to be secondary to the basic requirement that piles in liquefiable soils must be checked against Euler's buckling. However, this method can only consider one plastic hinge instead of two plastic hinges, which were observed at the interfaces of the liquefiable soil layer sandwiched between two no-liquefiable soil layers.

Meyerhosn (1994) proposed that piles subject to lateral spreads resulting from soil liquefaction might cause two distinct failure modes. The first one is lateral pile deflections induced by ground lateral spreads that may result in the pile reaching its bending capacity and hence develop a plastic hinge. Another failure mode is the combined action of lack of sufficient lateral support due to the reduced stiffness of the liquefied soil and the lateral deflection imposed on the pile, may result in pile buckling. Whether bending or buckling mode of a pile may develop depends primarily on the stiffness of the liquefied soil, length of pile exposed to liquefied soil, axial load imposed to pile, and bending stiffness of the pile. However, only bending failure analysis was conduced for the evaluated case histories.

Lin, *et al*. (2005) back studied possible failure modes of three case histories. Whether these piles were failed by either bending or buckling mode was re-evaluated. The design procedures suggested by Tokimatsu, *et al*. (1998) and by JRA (1996) were also used for case histories evaluation and compared to available observation results. Two bending failures and one buckling failure among the three studied cases were concluded.

In order to understand the performance of the pile during soil liquefaction with the numerical analyses, the paper uses the uncoupled numerical analysis to resolve this problem. First, the Winkler type model is used to simulate the soil-structure interaction. The Bouc-Wen model is used to mode soil behavior. At the same time, the Bouc-Wen model is also used to calculate the pile structure integrity while the pile fracture is triggered. Second, while considering the soil-structure interaction during the soil liquefaction event, another important factor is the change of the excess pore water pressure. To obtain this solution, the CYCLIC-1D (developed at the University of California at San Diego) is used to generate the acceleration and excess pore water pressure values within soils, however the possible effect of the existence of pile foundation is ignored, under the corresponding input earthquake motion. Then the values of excess pore water pressures at various depths can be combined with the Winkler model.

In order to verify this uncoupled approach, this paper also simulates the results of a centrifuge test and studies one real field case by the aforementioned method. Reasonable agreement was obtained between the predicted and the measured results.

Manuscript received September 4, 2006; revised October 31, 2006; accepted November 23, 2006.

[1] Professor (corresponding author), Department of Harbor and River Engineering National Taiwan Ocean University, Keelung 20224, Taiwan, R.O.C. (e-mail: sslin@mail.ntou.edu.tw).

[2] Graduate student, Department of Harbor and River Engineering National Taiwan Ocean University, Keelung 20224, Taiwan, R.O.C.

[3] Associate Researcher, Taiwan Construction Research Institute, Taipei County 251, Taiwan, R.O.C.

[4] Researcher, Taiwan Construction Research Institute, Taipei County 251, Taiwan, R.O.C.

2. UNCOUPLED MODELING

This study uses the Winkler model to simulate the soil-structure interaction caused by the earthquake motion. Considering the force equilibrium between the surrounding soil and the pile itself, the equation is described as Eq. (1).

$$E_P I_P \frac{\partial^4}{\partial x^4} w(x,t) + m \frac{\partial^2}{\partial t^2} w(x,t) = F_S(x,t) + F_d(x,t) \quad (1)$$

where $w(x, t)$ is the lateral pile displacement in various time step t; x is depth to the ground surface; m is element mass of pile; E_P is Young's Modulus of pile; I_P is moment of inertia of pile; $E_S(x, t)$ is non-linear soil reaction force; $E_d(x, t)$ is radiation damping force of pile. Two major components of Eq. (1) are the $E_S(x,t)$ and $E_d(x,t)$. In the following, these two parts are defined based on the soil modeling.

After the initiation of soil liquefaction, the lateral force produced by the soil movement may increase the bending moment. Furthermore, when the bending moment increases to a certain level, this may cause the material fracture that leads to the strength reduction. This study involves the pile fracture phenomenon that is described in the following section of moment-curvature relation of pile.

2.1 Soil Modeling

Based on the Bouc-Wen model, the force resulting from the nonlinear spring alone can be given as (Wen, 1985; Lin, *et al*., 2002)

$$F_S(x) = \alpha \cdot K \cdot w + (1-\alpha) \cdot K \cdot w_0 \cdot \varsigma(x) \quad (2)$$

where α is a parameter controls the post yielding stiffness; K is a reference stiffness; w is the pile deflection at the location of the spring; w_0 is the value of pile deflection that initiates yielding in the spring; and ς is a hysteretic dimensionless quantity that is governed by the following Eq. (3) (Wen, 1985; Lin, *et al*., 2002)

$$w_0 \dot{\varsigma} + \gamma \cdot |\dot{w}| \cdot \dot{\varsigma} \cdot |\varsigma|^{n-1} + \beta \cdot \dot{w} \cdot |\varsigma|^n - A \cdot \dot{w} = 0 \quad (3)$$

where A, β, γ and n are parameters that control the shape of the hysteretic loop and are chosen such that the shape of the loop is reasonable for the type of material considered. The maximum value of ς is given as

$$\varsigma = \left(\frac{A}{\beta + \gamma} \right)^{1/n}, \quad \text{when} \quad d\varsigma / dw = 0 \quad (4)$$

The spring reactions of the pile for cohesion-less soils were given by Badoni and Makris (1996) as

$$F_s(x) = \mu \cdot \gamma_s \cdot d \cdot \frac{1+\sin\phi_s}{1-\sin\phi_s} \cdot x \cdot \zeta(x) \quad (5)$$

where d is the pile diameter; ϕ_s is the angle of the soil internal friction; μ is a nonlinear hysteretic parameter; γ_s is the specific weight of the soil.

Another major concern of the soil liquefaction event is the initiation of the excess pore water pressure. Kagawa, *et al*. (1992) used a reduction factor F to describe the reducing the soil strength as follows.

$$F = (\sigma' / \sigma_0')^{\alpha_u} = (1-u)^{\alpha_u} \quad (6)$$

where α_u is the experiment parameter for sand is 0.5; u is the pore pressure ratio. By combining Eq. (6) with Eq. (5), Eq. (7) shows the non-linear soil reaction force F_S with the effect of the reduction form the pore water pressure generation.

$$F_S = (1-u)^{\alpha_u} \mu \gamma_s d \frac{1+\sin\phi_s}{1-\sin\phi_s} x \cdot \zeta \quad (7)$$

When the soil-structure interaction is subjected to the seismic force, the radiation damping should be considered. According to Badoni and Makris (1996), it can be described as Eqs. (8) and (9).

$$F_d = Q\, a_0^{-0.25} \rho_S V_S\, d\omega(\Delta w) \quad (8)$$

$$Q = 2\left[1 + \frac{3.4}{\pi(1-\nu_s)}\right]^{1.25} \cdot \left(\frac{\pi}{4}\right)^{0.75} \quad (9)$$

where ν_s is Poison's ratio of soil; a_0 is non-dimensional frequency dependent parameter $\left(a_0 = \frac{\omega d}{V_s}\right)$; ω is frequency; d is diameter of pile; V_s is shear velocity of soil; ρ_s is soil density; $(\Delta w) = w_0$ $(\Delta w > w_0)$ for the non-linear case; $(\Delta w) = \Delta w$ $(\Delta w \le w_0)$ for the linear case.

Under the effect of the excess pore water pressure, Eq. (9) can be re-written as Eq. (10).

$$F_d = \left[(1-u)^{1/4} + \frac{V_L u}{(V_s + V_p)}\right] Q\, a_0^{-0.25} \rho_S V_S\, d\omega(\Delta w) \quad (10)$$

where V_p is velocity of pressure; V_L is viscous velocity of liquefied soil. Transformation from frequency-dependent F_d to time-dependent F_d is detailed in Badoni (1997).

2.2 Moment-Curvature Relation of Pile

The Bouc-Wen model is also used to model moment-curvature relationship of the pile and is expressed as (Lin, *et al*., 2001)

$$M = \alpha_m (E_P I_P)\phi + (1-\alpha_m) M_y z \quad (11)$$

where M_y is the yield moment; ϕ is the curvature; α_m is a parameter controlling the rigidity of the pile after yielding; and z is the hysteretic parameter, which can be expressed as (Lin, *et al*., 2001)

$$\dot{z} = \left\{ A_M I_P - \left[B \cdot z^2 \{\text{sgn}(\dot{\phi} \cdot z) + 1\} \frac{1}{\phi_y} \right] \right\} \dot{\phi} \quad (12)$$

in which $\text{sgn}(\dot{\phi} \cdot z) = 1$ if $\dot{\phi} \cdot z > 0$; $\text{sgn}(\dot{\phi} \cdot z) = -1$ if $\dot{\phi} \cdot z < 0$; ϕ_y is the yielding curvature; and A_M and B is the parameters controlling the shape of the hysteretic loop.

For concrete piles, once the moment induced on the pile exceeds a certain magnitude, the moment of inertia of the pile may be reduced due to concrete cracking. A semi-empirical moment versus moment of inertia relationship is used in this paper (Lin, *et al*., 2001). The semi-empirical form is expressed as

$$I_{ef} = I^{I},\ (M < M_{cr}) \tag{13}$$

$$I_{ef} = I^{II} + (I^{I} - I^{II})\left(\frac{M_{cr}}{M}\right)^{3},\ (M_{cr} < M < M_{u}) \tag{14}$$

where I_{ef} is the effective moment of inertia; $I^{I} = I_p$, the moment of inertia of the non-cracked section; I^{II} is the moment of inertia of the completely cracked section where the reinforcement has reached the yield strength; M_{cr} is the bending moment corresponding to the beginning of cracking; and M_u is the bending moment corresponding to I^{II}.

In order to take into account the effects of finite size of plastic regions, the model chosen for this study is based on the global frame member model proposed by Roufaiel and Meyer (1987), in which the model was also successfully used for concrete pile analyses (Badoni, 1997). The element used is schematically illustrated in Fig. 1. The intermediate degree of freedoms can be factored out by the process of static condensation. The element stiffness matrix can be written as

$$[\hat{K}_b] = \begin{bmatrix}
12\frac{(E_pI_p)_i}{I_i^3} & 6\frac{(E_pI_p)_i}{I_i^2} & 0 & 0 & 12\frac{(E_pI_p)_i}{l_i^3} & 6\frac{(E_pI_p)_i}{l_i^2} & 0 & 0 \\
6\frac{(E_pI_p)_i}{I_i^2} & 4\frac{(E_pI_p)_i}{I_i} & 0 & 0 & -6\frac{(E_pI_p)_i}{l_i^2} & 2\frac{(E_pI_p)_i}{l_i} & 0 & 0 \\
0 & 0 & 12\frac{(E_pI_p)_j}{I_j^2} & -6\frac{(E_pI_p)_j}{I_j^2} & 0 & 0 & -12\frac{(E_pI_p)_j}{l_j^3} & 6\frac{(E_pI_p)_j}{l_j^2} \\
0 & 0 & -6\frac{(E_pI_p)_j}{I_j^2} & 4\frac{(E_pI_p)_j}{I_j} & 0 & 0 & -6\frac{(E_pI_p)_j}{l_j^2} & 2\frac{E_pI_p}{l_i} \\
-12\frac{(E_pI_p)_i}{I_i^3} & -6\frac{(E_pI_p)_i}{I_i^2} & 0 & 0 & 12\frac{(E_pI_p)_i}{l_i^3}+12\frac{E_pI_p}{l^3} & -6\frac{(E_pI_p)_i}{l_i^2}+\frac{E_pI_p}{l^2} & 12\frac{(E_pI_p)_j}{l^3} & 6\frac{(E_pI_p)_j}{l^2} \\
6\frac{(E_pI_p)_i}{I_i^2} & 2\frac{(E_pI_p)_p}{I_i} & 0 & 0 & -6\frac{(E_pI_p)_i}{l_i^2}+6\frac{(E_pI_p)}{l^2} & 4\frac{(E_pI_p)_i}{l_i}+4\frac{E_pI_p}{l} & -6\frac{(E_pI_p)_j}{l^2} & 2\frac{E_pI_p}{l} \\
0 & 0 & -12\frac{(E_pI_p)_j}{I_j^3} & -6\frac{(E_pI_p)_j}{I_j^2} & -12\frac{(E_pI_p)}{l^3} & -6\frac{E_pI_p}{l^2} & 12\frac{(E_pI_p)_j}{l_j^3}+12\frac{E_pI_p}{l^3} & 6\frac{(E_pI_p)_j}{l_j^2}-\frac{E_pI_p}{l^2} \\
0 & 0 & 6\frac{(E_pI_p)_j}{I_j^2} & 2\frac{(E_pI_p)_j}{I_j} & 6\frac{E_pI_p}{l^2} & 2\frac{E_pI_p}{l} & 6\frac{(E_pI_p)_i}{l_j^2}-\frac{E_pI_p}{l^2} & 4\frac{(E_pI_p)_j}{l_j}+4\frac{E_pI_p}{l}
\end{bmatrix} \tag{15}$$

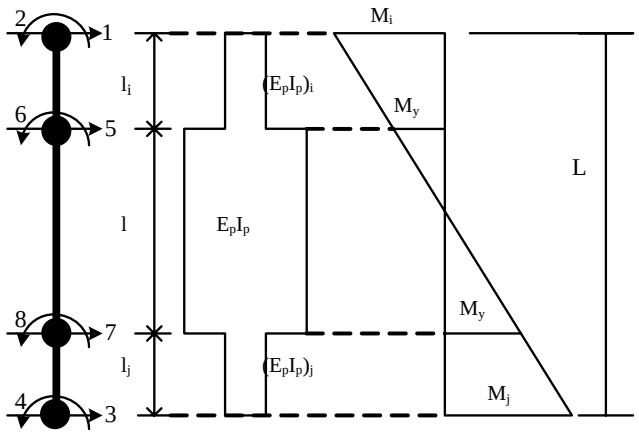

Fig. 1 Element used to model variable elasticity showing uncondensed of numbering and plastic zones (Badoni 1997)

which is defined by

$$\{F\} = [\hat{K}_b]\{Y\} \tag{16}$$

in which $\{Y\}$ and $\{F\}$ are the vectors of nodal displacement and nodal load, respectively. Set the nodal load values for the internal nodes to zero, the equation can be rewritten as

$$\begin{bmatrix} K_{bb} & K_{br} \\ K_{rb} & K_{rr} \end{bmatrix}\begin{bmatrix} y_b \\ y_r \end{bmatrix} = \begin{bmatrix} F_b \\ 0 \end{bmatrix} \tag{17}$$

in which the subscript r indicates the degrees of freedom to be condensed out. Hence, the modified element stiffness after condensation becomes

$$[K_b] = [K_{bb} - K_{br}K_{rr}^{-1}K_{rb}] \tag{18}$$

in which

$$[K_{bb}]=\begin{bmatrix} 12\dfrac{(E_pI_p)_i}{l_i^3} & 6\dfrac{(E_pI_p)_i}{l_i^2} & 0 & 0 \\ 6\dfrac{(E_pI_p)i}{l_i^2} & 4\dfrac{(E_pI_p)_i}{l_i} & 0 & 0 \\ 0 & 0 & 12\dfrac{(E_pI_p)_j}{l_j^3} & -6\dfrac{(E_pI_p)_j}{l_j^2} \\ 0 & 0 & -6\dfrac{(E_pI_p)_j}{l_j^2} & 4\dfrac{(E_pI_p)_j}{l_j} \end{bmatrix} \tag{19}$$

$$[K_{rr}]=\begin{bmatrix} 12\dfrac{(E_pI_p)_i}{l_i^3}+12\dfrac{E_pI_p}{l^3} & -6\dfrac{(E_pI_p)_i}{l_i^2}+6\dfrac{E_pI_p}{l^2} & -12\dfrac{E_pI_p}{l^3} & 6\dfrac{E_pI_p}{l^2} \\ -6\dfrac{(E_pI_p)_i}{l_i^2}+6\dfrac{E_pI_p}{l^2} & 4\dfrac{(E_pI_p)_i}{l_i}+4\dfrac{E_pI_p}{l} & -6\dfrac{E_pI_p}{l^2} & 2\dfrac{E_pI_p}{l} \\ -12\dfrac{E_pI_p}{l^3} & -6\dfrac{E_pI_p}{l^2} & 12\dfrac{(EI)_j}{l_j^3}+12\dfrac{E_pI_p}{l^3} & 6\dfrac{(E_pI_p)_j}{l_j^2}-6\dfrac{E_pI_p}{l^2} \\ -6\dfrac{E_pI_p}{l^2} & 2\dfrac{E_pI_p}{l} & 6\dfrac{(E_pI_p)_j}{l_j^2}-6\dfrac{E_pI_p}{l^2} & 4\dfrac{(E_pI_p)_j}{l_j}+4\dfrac{E_pI_p}{l} \end{bmatrix} \tag{20}$$

and

$$[K_{br}]=[K_{rb}]^T=\begin{bmatrix} -12\dfrac{(E_pI_p)_i}{l_i^3} & 6\dfrac{(E_pI_p)_i}{l_i^2} & 0 & 0 \\ -6\dfrac{(E_pI_p)_i}{l_i^2} & 2\dfrac{(E_pI_p)_i}{l_i} & -12\dfrac{(E_pI_p)_j}{l_j^3} & 6\dfrac{(E_pI_p)_j}{l_j^2} \\ 0 & 0 & -6\dfrac{(E_pI_p)_j}{l_j^2} & 2\dfrac{(E_pI_p)_j}{l_j} \end{bmatrix} \tag{21}$$

$(E_pI_p)_i$ and $(E_pI_p)_j$ in Eq. (11) are obtained from the moment-curvature relationships at the corresponding ends.

The plastic region lengths l_i and l_j for ends i and j are obtained as

$$l_i=\frac{M_i-\mathrm{sgn}(M_i)M_{cr}}{M_i+M_j}L \tag{22}$$

and

$$l_j=\frac{M_j-\mathrm{sgn}(M_j)M_{cr}}{M_i+M_j}L \tag{23}$$

Since the plastic zone length depends on the end-moments at the current loading increment, an iterative technique is required in which l_i is progressively refined until convergence is reached according to the calculating steps listed below:

For each loading increment (Badoni 1997):

(a) Calculate l_i, l_j, $(E_pI_p)_i$ and $(E_pI_p)_j$ for all yielding elements based on the end moments at the previous loading increment;

(b) Calculate the modified element stiffness matrix $[K_b]$, given in Eqs. (15) and (16), for these elements and assemble the global effective stiffness matrix and load vectors;

(c) Input nodal forces $\{F_b\}$

$$\{Y_b\}=[K_b]^{-1}\{F_b\} \tag{24}$$

and calculate nodal displacements $\{Y\}$

$$\{Y_r\}=-[K_{rr}]^{-1}[K_{br}]^T\{Y_b\} \tag{25}$$

(d) Update element end-moments based on new nodal vector;

(e) Recalculate l_i, l_j, $(E_pI_p)_i$ and $(E_pI_p)_j$ and check for convergence. Repeat until convergence is achieved.

2.3 Numerical Procedures for Uncoupled Analysis

(a) Apply the CYCLIC-1D program to simulate the ground response and compute the values of acceleration and excess pore water pressure time histories at various depths;

(b) Substitute the acceleration and excess pore water pressures data obtained from procedure (a) into Winkler model of Eq. (1);

(c) Calculate the lateral displacement and bending moment at the corresponding depth of pile from procedure (b).

3. CENTRIFUGE TESTINGS

In order to verify the accuracy of the materials modeling

proposed in this paper, the analytical results will be compared with the measured data from the centrifuge testing results. Abdoun, *et al*. (2003) presented the results of the centrifuge testing that simulates a single pile sustaining the lateral spreading force from the soil liquefaction. In this study, three centrifuge test cases are compared.

Case A

As shown in Fig. 2, the dimension of the box is 45.72 m × 25.4 m × 26.39 m. The embedded model pile is 20 cm long with diameter of 0.95 cm and the soil material properties are shows in the Table 1. This entire assemble is tested under the gravity value of 50 g. Under such gravity, it can simulate a full-sized pile of 10 m in length with 47.5 cm in diameter. To test the soil liquefaction-induced lateral spreading effect, the layout of the model including three layers of soils:

Top layer: 2 m cemented sand with 34.5° of friction angle and 5.1 kPa of cohesion.

Middle layer: 6 m liquefiable sand (Nevada sand) with relative density of 40%, dry unit weight of 17.33 kN/m^3 ~ 13.87 kN/m^3.

Bottom layer: 2 m cemented sand with the same properties of the top layer.

(Note: the dimension shown above is the prototype model.)

During the testing, the bottom of the box is applied with an excitation to simulate the earthquake motion. The excitation has frequency of 20 Hz, maximum magnitude of 0.3 g, and 40 cycles. In order to simulate the effect of lateral spreading, the entire box is tilted by 4.8°. Free head and free tip pile boundary conditions are considered in the numerical analysis.

Case B

As shown in Fig. 3, the layout and the input motion of the Case B are the same as those of Case A. The major difference is the prototype dimension of pile is 8 m, in which the bottom of the pile does not extend into the bottom non-liquefied layer. Free head and free tip pile boundary conditions are considered in the numerical analysis.

Table 1 Soil material properties for Centrifuge Testing Model (after Abdoun, *et al*. 2003)

Nevada sand		Relative density, D_r (%)	40
		D_{10} (mm)	0.09
		D_{50} (mm)	0.15
		Specific gravity, G_s	2.67
		Max. void ratio, e_{max}	0.887
		Min. void ratio, e_{min}	0.511
		Max. dry unit wet., r_{dmax} (kN/m^3)	17.33
		Min. dry unit wet., r_{dmin} (kN/m^3)	13.87
		Permeability at 1 g for D_r = 40% (m/s)	6.6×10^{-5}
Cemented sand		ϕ (°)	34.5
		C (kPa)	5
Pile	Shear box	Length, L(m)	20
		Diameter (cm)	0.95
		EI (kN-m)	–
		Gravity value (g)	50
	Prototype	Length, L(m)	10
		Diameter (cm)	47.5
		EI (kN-m)	8000
		Gravity value (g)	–

Case C

As shown in Fig. 4, input motion of the Case C are the same as those of Case A. However, the major difference is the soil profiles. In Case C, there is no surface layer of the slightly cemented sand. Free head and free tip pile boundary conditions are considered in the numerical analysis.

To verify the accuracy of the materials model proposed in this paper, the verification procedure includes two steps, including CYCLIC-1D simulation and the materials modeling calculation. The parameters used for the materials model are shows in the Table 3.

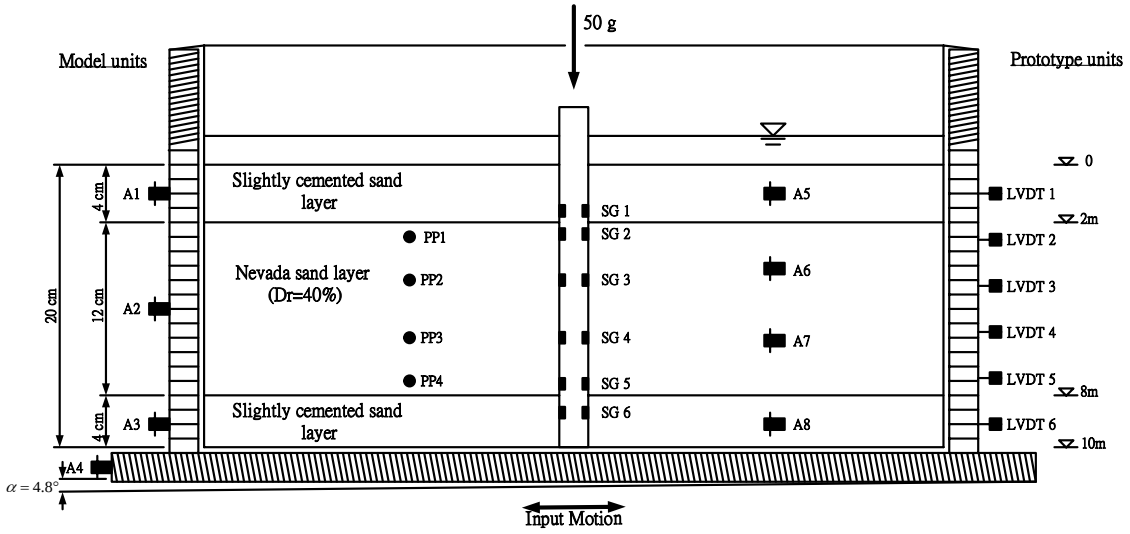

Fig. 2 Centrifuge testing model, Case A (after Abdoun, *et al*., 2003)

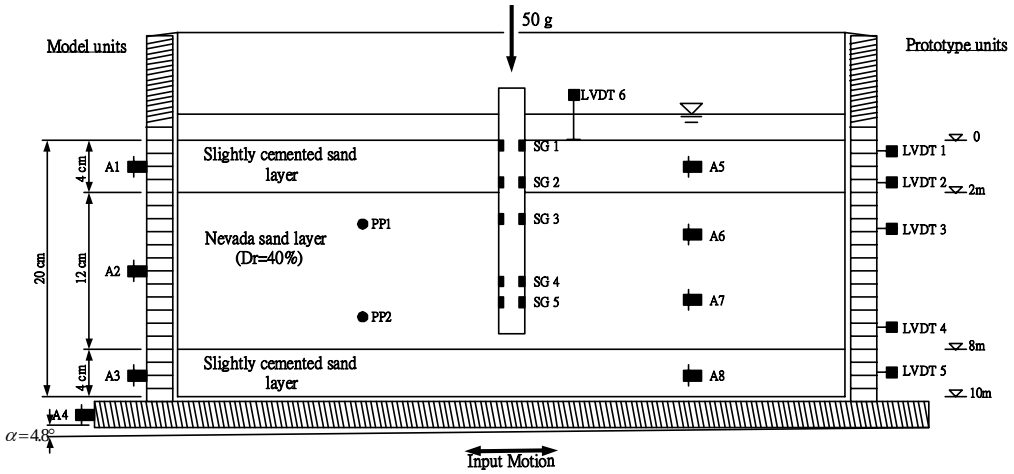

Fig. 3 Centrifuge testing model, Case B (after Abdoun, *et al*., 2003)

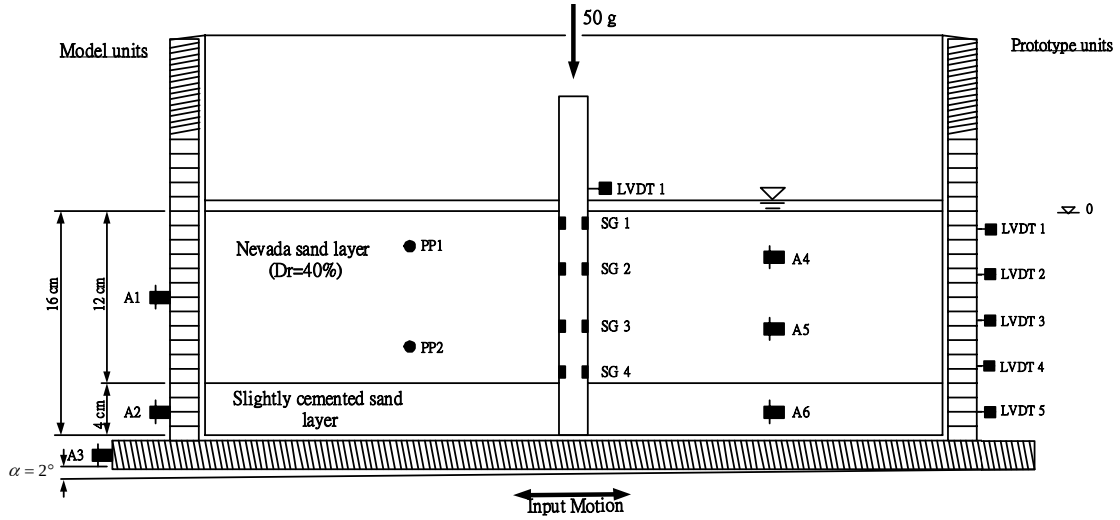

Fig. 4 Centrifuge testing model, Case C (after Abdoun, *et al*., 2003)

Table 2 Material properties used for the building in Mikagehoma, Japan (Tokimatsu 2003)

Back studied case	
Pile	
E_pI_p (kN-m^2)	5000
M_{cr} (kN-m)	12
M_y (kN-m)	75
M_u (kN-m)	100
ϕ_y (1/m)	0.015
Soil	
Upper non-liquefied layer	
depth (m)	0.0 ~ 1.5
γ_s (kN/m^3)	16.5
ϕ (°)	32
Middle (or upper) liquefied layer	
depth (m)	1.5 ~ 14.0
γ_s (kN/m^3)	12.5
ϕ (°)	25
Bottom non-liquefied layer	
depth (m)	14.0 ~ 23.0
γ_s (kN/m^3)	18.5
ϕ (°)	40

3.1 CYCLIC-1D Simulation

CYCLIC-1D was developed in the University of California at San Diego (Elgamal, *et al*., 2002). This program aims to solve soil liquefaction-induced lateral spreading problems. By providing the soil properties and soil profiles, it can estimate several soil responses (*e.g.,* acceleration, spectrum, excess pore water pressure, *etc*.) under the effect of the base motion. For further information, please access http://cyclic.ucsd.edu/index.html for details.

In this step, this study uses CYCLIC-1D to simulate the acceleration and pore water pressure time histories within various depths of the prototype test, including depth of 1m, 4m, 6m, and 9m. Figures 5 and 6 show the results of Case A; Fig. 7 shows the results of Case B and Fig. 8 shows the results of Case C. Note that the acceleration time histories excited at the bottom of the box of Cases A, B, and C are the same.

The data generated in this step will be implemented with the materials modeling to estimate the lateral displacement and bending moment at the corresponded depth of pile.

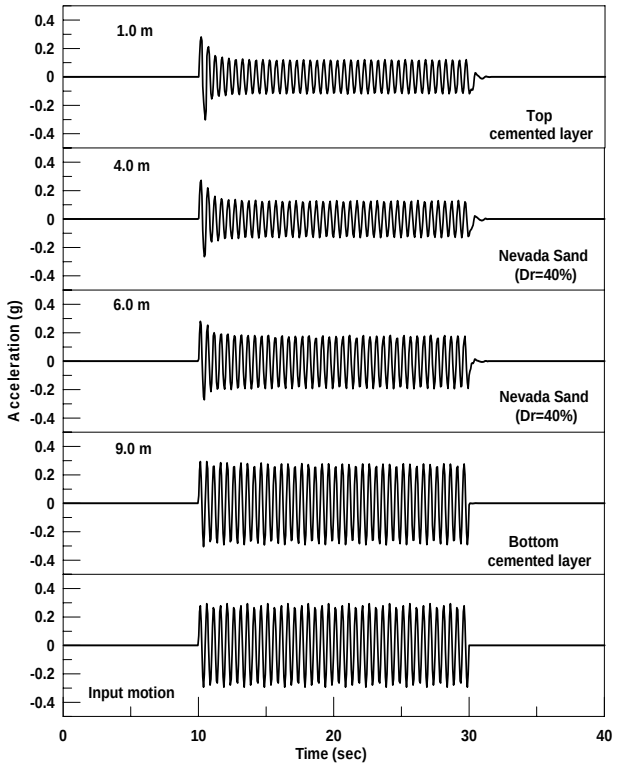

Fig. 5 CYCLIC-1D simulation of acceleration time histories at various depths of Case A

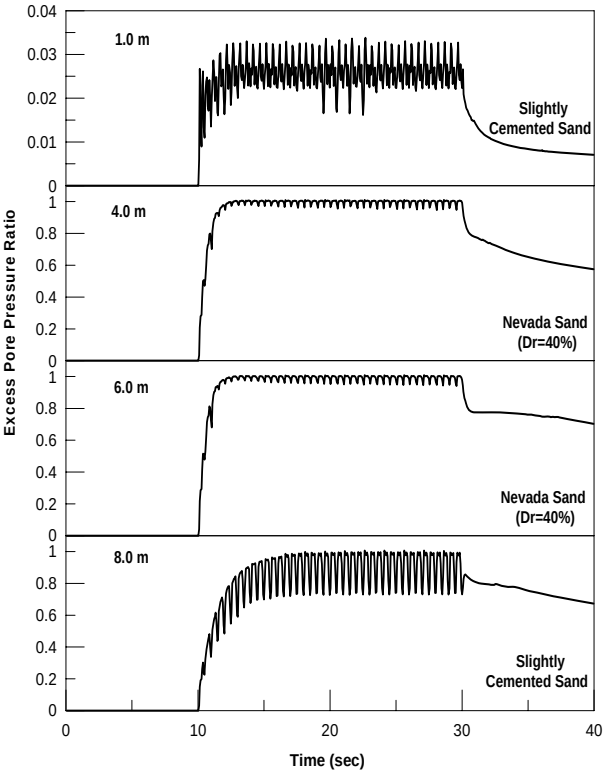

Fig. 7 CYCLIC-1D simulation of pore water pressure time histories at various depths of Case B

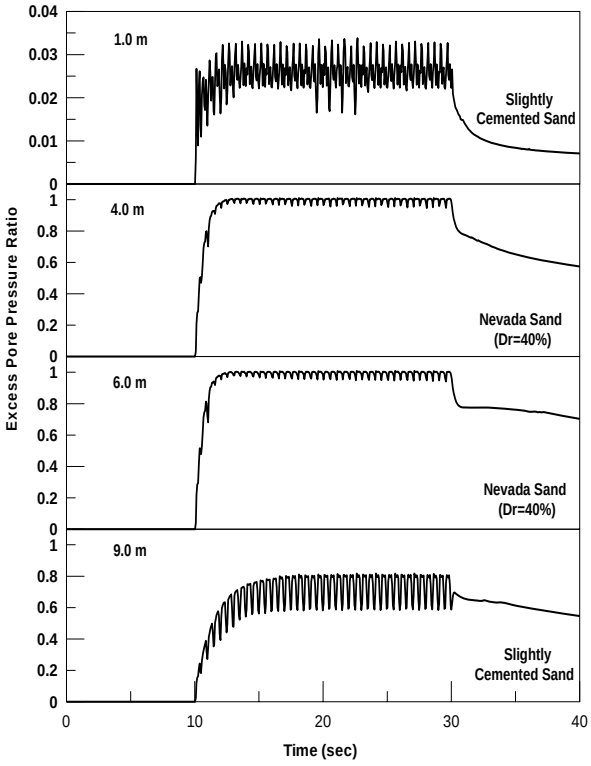

Fig. 6 CYCLIC-1D simulation of pore water pressure time histories at various depths of Case A

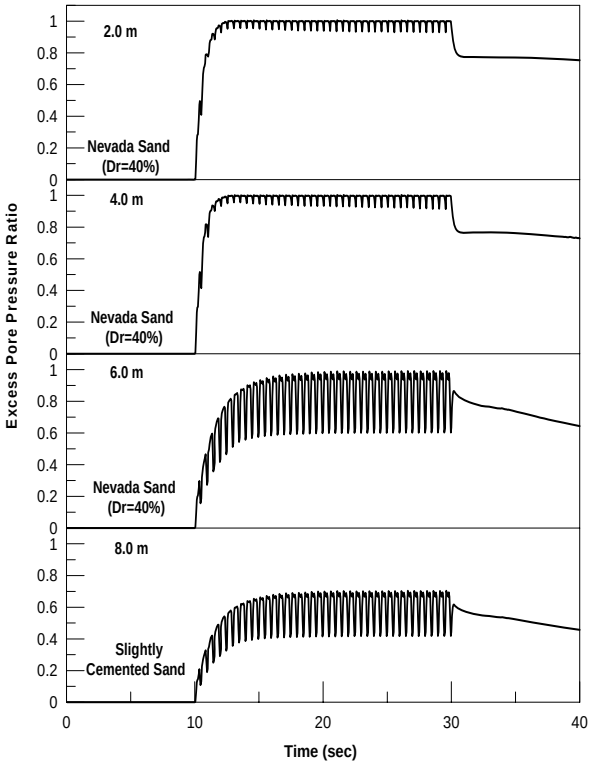

Fig. 8 CYCLIC-1D simulation of pore water pressure time histories at various depths of Case C

3.2 Materials Modeling Calculation

Combined with the results from the CYCLIC-1D, the materials model estimates the lateral displacement and the bending moment of the pile. For the Case A study, Figs. 9 and 10 show the calculation results of pile lateral displacement and bending moment, respectively. Figures 11 and 12 show the parametric study results of bending moment of pile with or without pore water pressure consideration at various time steps and at various ground inclination angles, respectively. In general, due to the soil liquefaction effect at the middle layer, it produces the lateral movement among the top and middle layer. However, the bottom layer with non-liquefied soils that remain relatively intact. This action of lateral movement that produces force to apply on the pile, which also carry the upper part of pile to move with soil. The lower part of pile, on the other hand, remain relatively unmovable. This phenomenon produces large bending moment to concentrate at the boundary between the middle liquefied layer and the bottom non-liquefied layer.

Compared with the Case A study, Fig. 13 shows the bending moment of pile in Case B and Fig. 14 shows the bending moment of pile at various ground inclination angles. Even though the pile does not extend into the bottom non-liquefied layer, it still shows a concentration of bending moment between the top non-liquefied layer and the middle liquefied layer.

Table 3 Parameters used for the Uncoupled Numerical Analysis

Parameter		Centrifuge testing	A building in Mikagehoma
Shape parameters of hysteretic loop	A	4.1	3
	β	0.09	0.5
	γ	0.09	0.5
	n	1.0	1.0
Nonlinear hysteretic parameter, μ		6.0	3
Frequency, ω (1/sec)		2.0	1.6
Shape parameters of moment-curvature hysteretic loop	A_M	8	8
	B	65	1
Yielding stiffness parameter, α		0.95	0.3

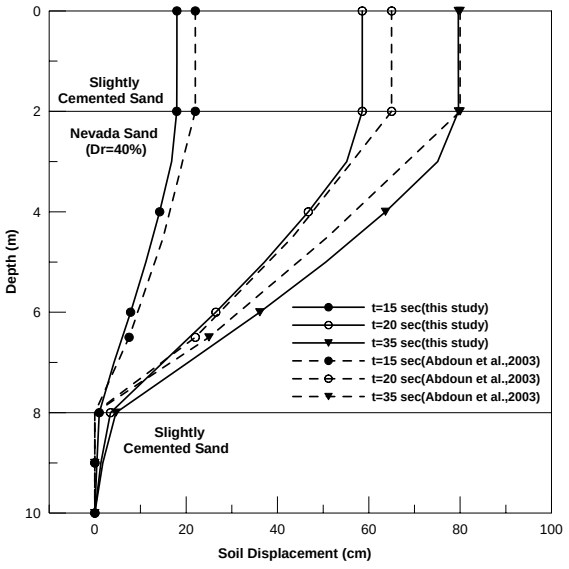

Fig. 9 Calculation of lateral displacement of prototype pile at various time steps of Case A

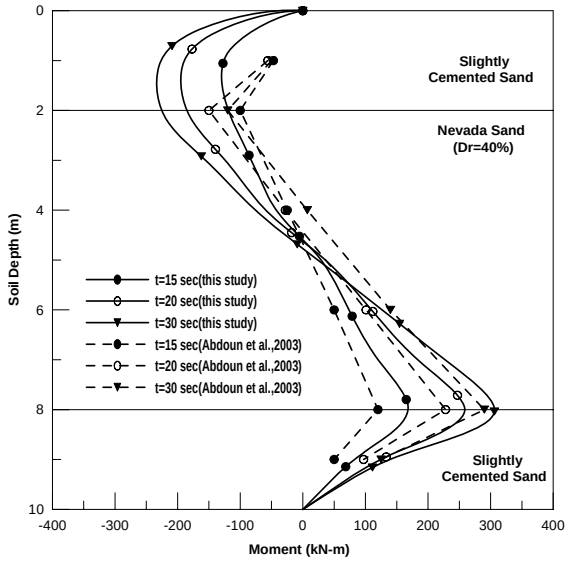

Fig. 10 Calculation of bending moment of prototype pile at various time steps of Case A

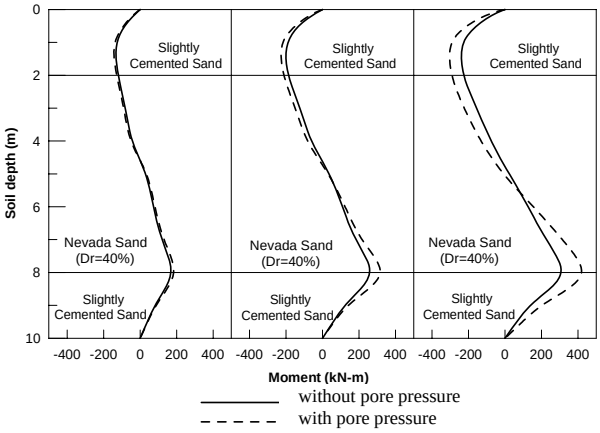

(a) 15 sec (b) 20 sec (c) 30 sec

Fig. 11 Calculation of bending moment of prototype pile with or without pore water pressure consideration at various time steps of Case A

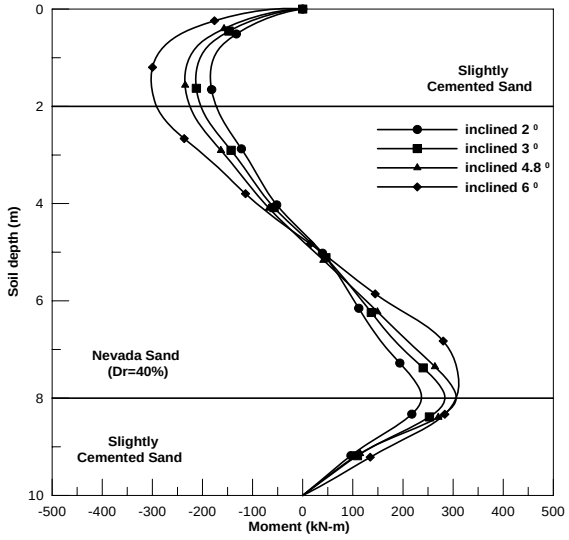

Fig. 12 Calculation of bending moment of prototype pile at various inclination angles of Case A

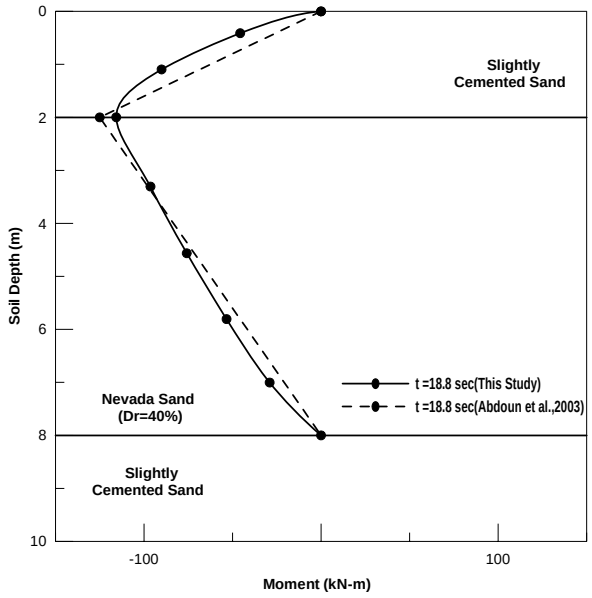

Fig. 13 Calculation of bending moment of prototype pile at various time steps of Case B

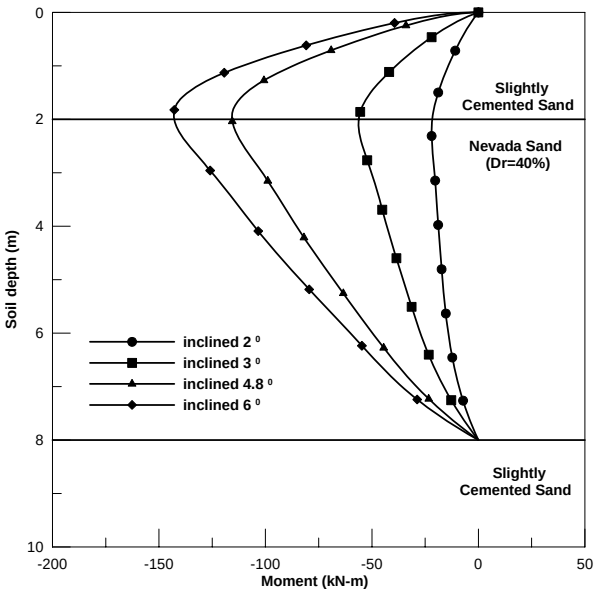

Fig. 14 Calculation of bending moment of prototype pile at various inclination angles of Case B

In the Case C, Figs. 15 and 16 show the calculation results of pile lateral displacement and bending moment, respectively. Figure 17 shows the bending moment of pile at various inclination angles. Unlike Case A, due to lack of the surface cemented sand, the displacement and bending moment distributions are different. However, the maximum values still concentrated at the boundary between the liquefied layer and the bottom fixed layer.

By compared with the actual measured data collected from the centrifuge data, all three cases show a good agreement between the calculations results and the actual measured data.

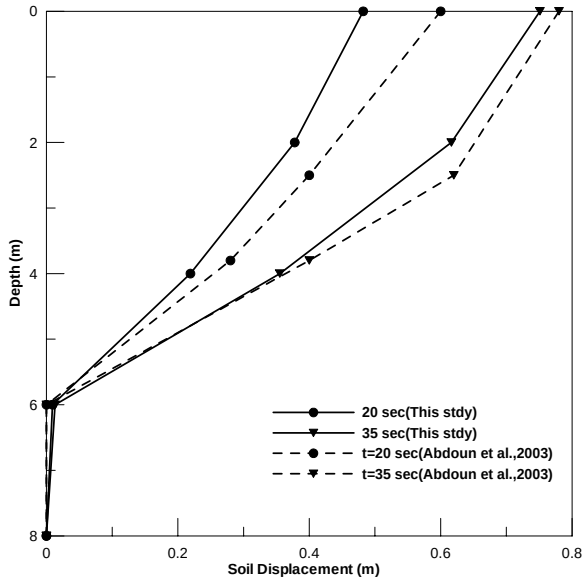

Fig. 15 Calculation of lateral displacement of prototype pile at various time steps of Case C

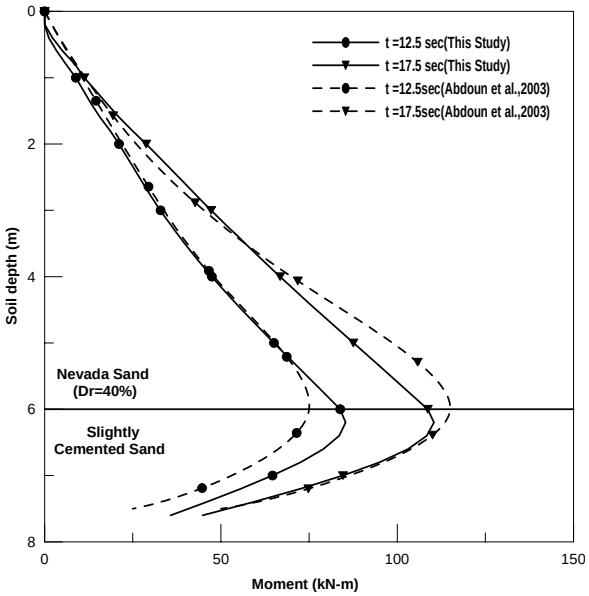

Fig. 16 Calculation of bending moment of prototype pile at various time steps of Case C

4. A BUILDING IN MIKAGEHOMA, JAPAN (Tokimatsu 2003)

A case history of 35 cm diameter and 23 m long pre-stressed high strength concrete piles supporting a four-story building in Mikagehama reviewed by Tokimatsu (2003) who used the pseudo-static analysis method. After the 1995 Kobe earthquake was also back studied via the method by Lin, *et al*. (2005) for its possible failure mode. The moment curvature properties of the piles and other soil properties are given in Table 2. In the calculation procedure, it also considers the possible concrete cracking effect when the bending moment exceeding the maximum value. Figures 18 and 19 shows the simulation of acceleration and pore water pressure time histories at various depths, respectively. Figures 20 and 21 show the lateral displacement and bending

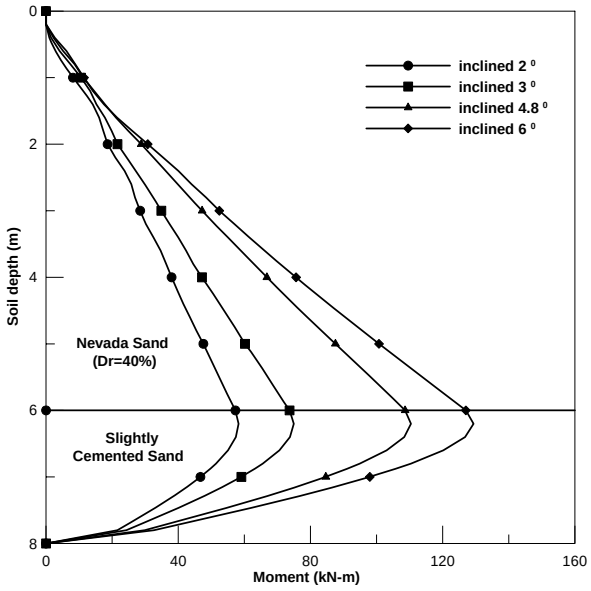

Fig. 17 Calculation of bending moment of prototype pile at various inclination angles of Case C

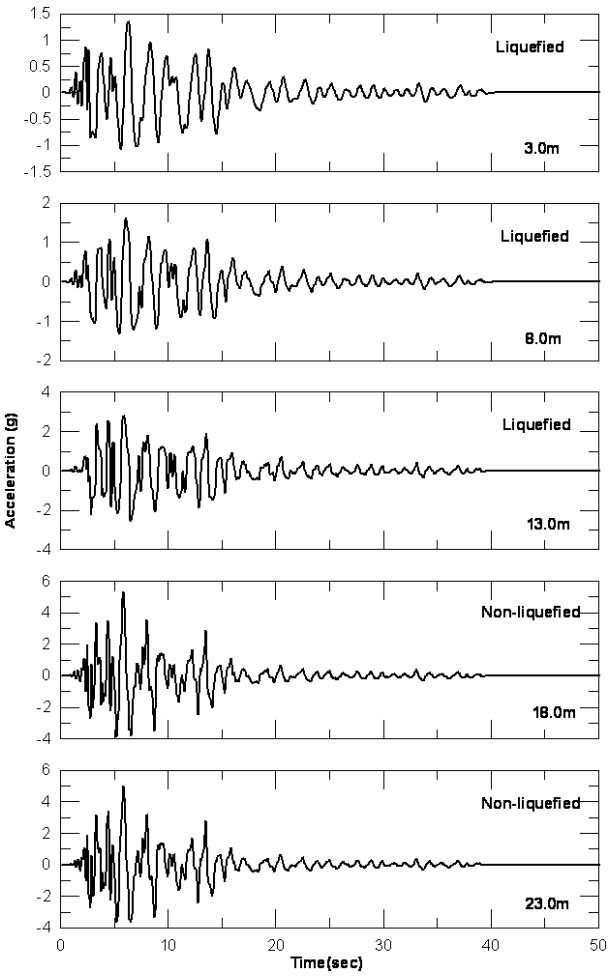

Fig. 18 CYCLIC-1D simulation of acceleration time histories at various depths of the building in Mikagehoma, Japan (Tokimatsu, 2003)

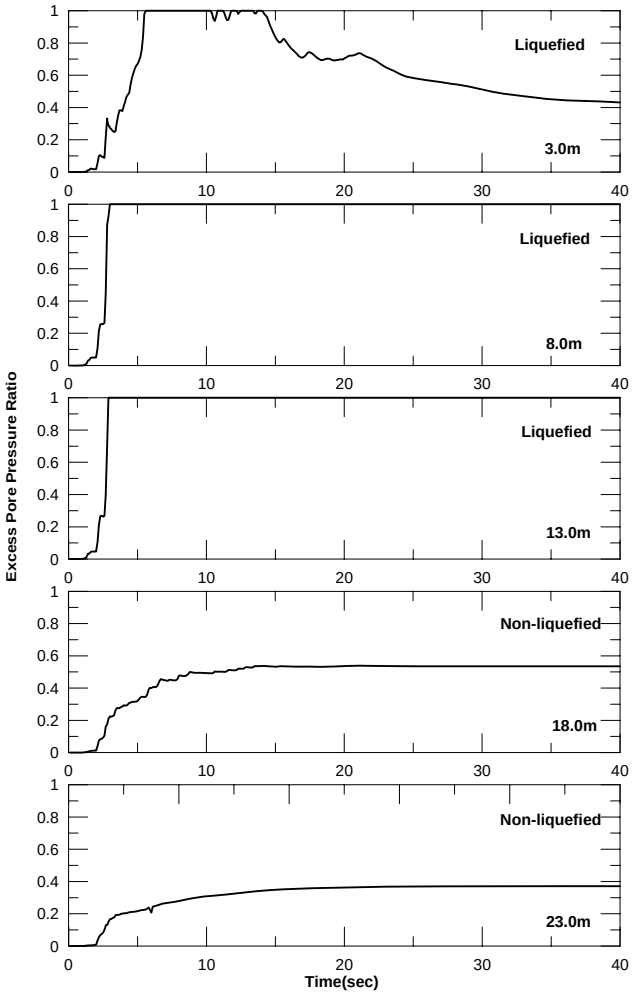

Fig. 19 CYCLIC-1D simulation of pore water pressure time histories at various depths of the building in Mikage-homa, Japan (Tokimatsu, 2003)

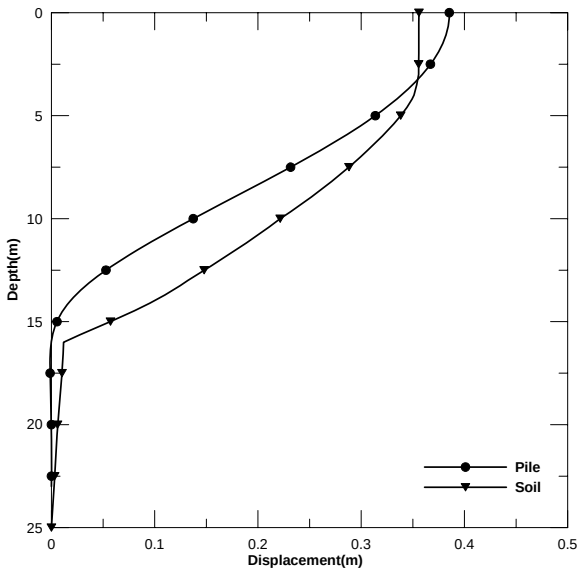

Fig. 20 Calculation of lateral displacement of pile and soil at various depth of the building in Mikagehoma, Japan (Tokimatsu, 2003)

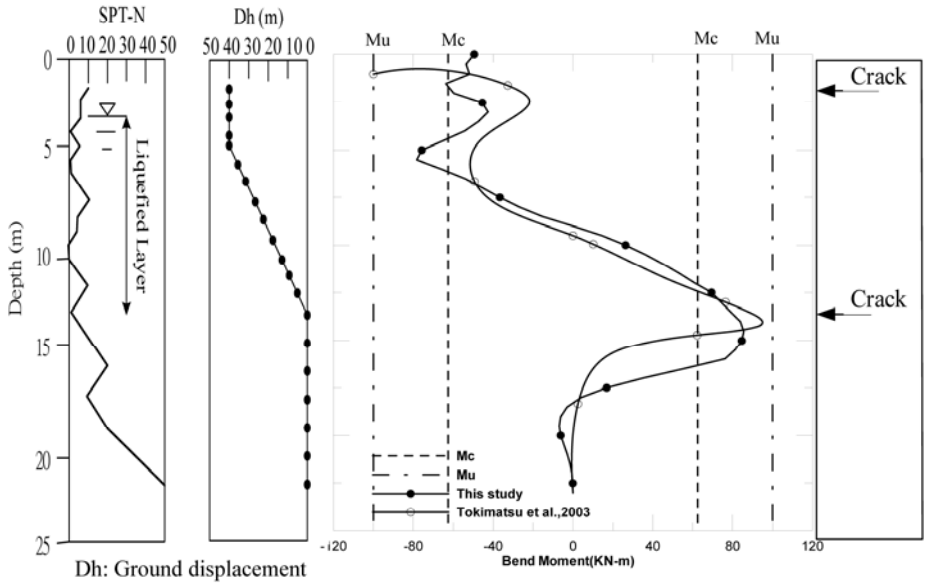

Fig. 21 Calculation of bending moment of pile at various depth of the building in Mikagehoma, Japan (Tokimatsu, 2003)

moment of pile at various depth. Field survey showed that the piles cracked near the pile head and near the bottom of the fill causing tilting of the building, as shown in Fig. 21. The predicted maximum moment locations match well with the observed concrete crack locations of the pile.

5. SUMMARY AND CONCLUSIONS

In this paper, a decoupled numerical approach was used to study the ground lateral spread effects on single piles. The Winkler model was used to simulate the soil-structure interaction between the pile and the surrounding liquefied and non-liquefied soils. The Bouc-Wen model, which had previously been successfully used to represent static and cyclic soil properties for pile analysis (Lin, *et al*., 2001; Badoni and Makris, 1996), has been extended here to model the effects of concrete cracking on the pile performance caused by ground lateral spreads.

Three centrifuge tests produced by Abdoun, *et al*. (2003) and one real field case (Tokimatsu, 2003) were used to verify the proposed model. The CYCLIC-1D (developed at the University of California at San Diego) is used to generate the acceleration and excess pore water pressure time histories during the soil liquefaction-induced lateral spreading event. Finally, the entire uncoupled numerical analyses approach combines the results of the CYCLIC-1D and the Winkler model to estimate the lateral displacement and bending moment of the single pile under the effect of lateral spreading force. The results show a good agreement between the measured and calculated lateral displacement and bending moment of pile.

ACKNOWLEDGEMENTS

This study was supported by the National Science Council and MOTC, Taiwan, under grant number NSC 92-2211-E-019-007 and MOTC-STAO-94-01, respectively. Grateful appreciation is expressed for this support.

REFERENCES

Abdoun, T., Dobry, R., O'Rourke, T. D., and Goh, S. H. (2003). "Pile response to lateral spreads: centrifuge modeling." *Journal of Geotechnical and Geoenvironmental Engineering*, ASCE, 129(10), 869-878.

Badoni, D. and Makris, N. (1996). "Nonlinear response of single piles under lateral inertial and seismic loads." *Soil Dynamics and Earthquake Engineering*, 15, 29-43.

Badoni, D. (1997). "Nonlinear response of pile foundation-superstructure systems." Ph.D. Dissertation, Department of Civil Engineering, University of Notre Dame, Indiana, USA.

Bhattacharya, S., Madabhushi, S.P.G., and Bolton, M.D. (2004). "An alternative mechanism of pile failure in liquefiable deposits during earthquakes." *Geotechnique*, 54(3), 203-213.

Elgamal, A., Yang, Z., Parra, E. and Ragheb, A. (2002). "Cyclic 1D-An internet-based nonlinear finite element program for execution of one-dimensional site amplification and liquefaction simulations." University of California at San Diego, http://cyclic.ucsd.edu/index.html for details.

Hamada M. (1992). "Large ground deformations and their effects on lifelines: 1964 Niigata Earthquake in case studies of liquefaction and lifeline performance during past earthquakes." Japanese Case Studies, Technical Report, NCEER-92-0001, NCEER, Buffalo, NY, (1), 3.1-3.123.

Hwang, J. H., Yang, C. W., Chen, C. H. (2003). "Investigations on soil liquefaction during the Chi-Chi earthquake." *Soils and Foundations*, 43(6), 107-123.

Japanese Road Association (1996). *Specifications for Highway Bridges, Part V, Seismic Design*.

Kagawa, T., Taji, Y., Sato, M., and, Minowa, C. (1992). "Soil-pile-structure interaction in liquefying sand from large-scale shaking-table tests and centrifuge tests." *Analysis and Design for Soil-Pile-Structure Inter Actions*, GSP 70, 69-84.

Lin, S. S., Liao, J. C., Yang, T. S., and Juang, C. H. (2001). "Nonlinear response of single concrete piles." *Geotechnical Engineering Journal*, 32(3), 165-175.

Lin, S. S., Liao, J. C., Liang, T. T., and Juang, C. H. (2002). "Use of Bouc-Wen model for seismic analysis of concrete piles." *Deep Foundations 2002*, GSP 116, ASCE, 372-384.

Lin, S. S., Tseng, Y. J., Chiang, C. C., and Hung, C. L. (2005) "Damage of piles caused by lateral spreading-back study of three cases." *Seismic Performance and Simulation of Pile Foundations in Liquefied and Laterally Spreading Ground*, GSP 145, ASCE, 121-133.

Meyersohn, W. D. (1994). "Pile response to liquefaction-induced lateral spread." Ph.D. Dissertation, Cornell University, USA.

Roufaiel, M.S.L. and Meyer, C. (1987). "Analytical modeling of hysteretic behavior of R/C frames." *Journal of Structural Engineering*, ASCE, 113(3), 429-444.

Tokimatsu, K., Oh-oka, H., Satake, K., Shamoto, Y., and Asaka, Y. (1998). "Effects of lateral ground movements on failure pathenns of piles in the 1995 Hygoken-Nambu earthquake." *Geotechnical Earthquake Engineering and Soil Dynamics*, 3, 1175-1186.

Tokimatsu, K. (2003). "Behavior and design of pile foundations subjected to earthquakes." Keynote Speech, *12th Asia Regional Conference on Soil Mechanics and Geotechnical Engineering*, Singapore, 2, 1065-1096.

Wen, Y. K. (1985). "Response and damage of hysteretic systems under random excitation." *Proceedings of 4th International Conference on Structural Safety and Reliability*, 1, 291-300.